

Strain measurement in diacetylene-containing copolymers using Raman spectroscopy

X. HU, R. J. DAY, J. L. STANFORD, R. J. YOUNG*

Polymer Science and Technology Group, Manchester Materials Science Centre, UMIST and University of Manchester, Manchester M1 7HS, UK

Rigid diacetylene-containing block copolymers are shown to have Raman spectra similar to those of polydiacetylene single crystals. The vibrational frequencies of certain main-chain Raman-active modes of the copolymers are sensitive to deformation which enables strain measurement to be made by following the shift in the Raman band positions. Measurements of the stress concentrations around defects in copolymer specimens during deformation have been carried out using Raman spectroscopy and they have been compared with theoretical analyses of stress concentrations. There is good agreement between the theoretical and experimental measurements and it has been demonstrated that the use of Raman spectroscopy allows the measurement of stress or strain in complex situations for which no theoretical solutions exist.

1. Introduction

The Raman band positions in the Raman spectra of many materials, particularly highly oriented fibres, are known to shift significantly, generally to lower frequencies, when they are subjected to tensile deformation [1–10]. This shift arises because the applied macroscopic deformation is transformed directly into deformation of the covalent bonds in polymer chain backbones. The consequent changes in bond lengths and bond angles lead to shifts in the vibrational frequency of a particular Raman-active band. Of the polymers studied so far, polydiacetylene single crystals were shown to have Raman bands with the highest strain sensitivities, with the $C\equiv C$ triple stretching band shifting by -20 cm^{-1} per 1% strain [1–3]. Furthermore, Raman spectroscopy has also enabled *in situ* measurements of strain in fibres in composites with transparent matrices [5].

For there to be appreciable Raman band shifts, it is essential that there is deformation of the covalent bonds in the polymer backbones. Hence, the most successful materials for Raman deformation studies have been high-modulus, highly-oriented fibres, such as poly(*p*-phenylene terephthalamide) [4–6], ultra-high molecular weight polyethylene (UHMW-PE) [7–9], poly(*p*-phenylene benzobisthiazole) (PBT) [10] and poly(*p*-phenylene benzobisoxazole) (PBO) [11]. Such materials gain their excellent mechanical properties from macroscopic deformation being translated through their highly oriented structures into direct molecular stretching.

Studies of the effect of deformation upon the Raman spectra of less-oriented conventional polymers have

met with only limited success. For example, small but measurable band shifts have been obtained for hot-drawn poly(ethylene terephthalate) (PET) films [12], nylon and polypropylene [13, 14]. However, the shifts are often less than -1 cm^{-1} even at the yield stress of the material, whereas the shifts obtained for the highly oriented polymers can be typically over $-5\text{ cm}^{-1}/\%$ strain. This is understandable because in the conventional polymers only a small fraction of the macroscopic strain leads to deformation of the polymer backbone; the rest being taken up by molecular uncoiling, reptation or rotation about single bonds.

Although the majority of the Raman deformation studies reported so far have been confined to the study of high-modulus fibres and composites, it would be desirable to undertake similar investigations upon elastically isotropic polymers because an understanding of the deformation of such materials is equally, if not more important. One way forward is to incorporate polydiacetylene moieties with strain-sensitive Raman bands into multiphase copolymer systems which can be either glassy or elastomeric in nature [15–17]. The preparation and systematic characterization of these diacetylene-containing copolymers has been described elsewhere [15, 16]. The mechanical and opto-mechanical behaviour of these copolymers have also been studied in detail in relation to the molecular deformation in the polydiacetylene units [16, 17]. In the present paper, the strain dependence of Raman band frequencies in a rigid diacetylene-containing copolymer will be further discussed and, in particular, the use of Raman microscopy as an optical strain probe in the copolymer is reported in detail.

* Author to whom all correspondence should be addressed.

Examples are given which demonstrate the potential applications of these materials as novel optical strain sensors.

2. Experimental procedure

2.1. Materials

A rigid, glassy diacetylene-containing segmented copolyurethane with Young's modulus of about 2 GPa was prepared using a two-stage process. A linear segmented copolymer precursor was synthesized via a one-shot bulk polymerization process to give a material with diacetylene monomer units situated in the hard segments. It was synthesized using 4,4'-diphenylmethane diisocyanate (49.1 g), 2,4-hexadiyne-1,6-diol (10.2 g), polypropylene glycol with number average molar mass, $M_n \approx 400 \text{ g mol}^{-1}$ (38.8 g), and dipropylene glycol (1.94 g). The copolymer obtained contains 33% diacetylene hard segments. It was polymerized and cast into sheets at 60 °C. The full details of its synthesis and chemical structure have been described in a previous publication [15]. Transmission electron microscopic examination of ultra-microtomed sections has shown that these hard segments aggregate to form spherulitic domains which are distributed uniformly throughout the matrix phase [15]. Subsequent thermal treatment induces the cross-polymerization of the diacetylene units into polydiacetylene moieties [15]. This process is similar to the solid-state topochemical reaction in diacetylene single-crystal analogues. The polymer used in this present study was cross-polymerized by heating for 40 h at 100 °C. The polydiacetylene chains formed *in situ* act as Raman-active optical centres, chemical cross-links and also as mechanical reinforcements in a cross-polymerized copolymer [15–17]. Details of the synthesis procedure and structure/morphology/property relationships in these copolymers have been discussed in detail elsewhere [15–17].

2.2. Deformation analysis using Raman microscopy

Raman spectra of the copolymers were obtained using a 10 mW He–Ne laser with a wavelength of 632.8 nm as the excitation source. The laser beam was focused to a 2 μm spot on the sample surface through a $\times 40$ objective lens with a numeric aperture of 0.65 using a modified Nikon optical microscope. The scattered light was collected using 180° back-scattering geometry with the same objective lens and then focused on the entrance slit (0.4 mm) of a Spex 1403 double monochromator. A charge-coupled device camera, CCD (Wright Instruments), cooled with liquid nitrogen was employed as the detector which was found to have low noise, high sensitivity and high efficiency. Hence, the typical scanning time in this work was 10 s for a spectral window of 40 cm^{-1} . The Raman peaks were curve-fitted into a Gaussian profile and the absolute values of Raman band frequencies could be determined with an accuracy of $\pm 5 \text{ cm}^{-1}$ while strain-induced frequency shifts could be measured to at least ten times better accuracy.

Copolymer bulk sheets (2.5 mm thick) were machined into miniature dumb-bell specimens, 10 mm wide and 40 mm long in the gauge length region. The strain dependence of the frequency of the C \equiv C triple-bond stretching Raman band was determined by *in situ* tensile deformation of the copolymer specimens under the Raman microscope using a miniature materials tester (Polymer Laboratories). The specimens were stretched step-wise at a speed of 1 mm min^{-1} in steps of about 0.1% strain. Raman spectra were then obtained at various strain levels. A resistance strain gauge, attached to each specimen using a special adhesive M-Bond 200 (Micro-Measurements Group Inc.), was used to measure the strain to an accuracy of $\pm 0.002\%$. In all of the deformation experiments, the incident laser was polarized parallel to the tensile axis and the Raman band of the C \equiv C triple-bond stretching mode was used as the diagnostic band throughout. Experiments were carried out to determine the concentrations of stress around defects in the copolymer samples. Specimens with defects, such as a central hole or a single-edge notch, were deformed and Raman spectra were obtained from different positions in the vicinity of the defects. Strain mapping and point-to-point strain measurements were also performed using the Raman microprobe.

3. Results and discussion

3.1. Raman spectroscopy

The Raman spectrum in the range 300–2400 cm^{-1} for the cross-polymerized copolymer shown in Fig. 1 is strikingly similar to those obtained for polydiacetylene single crystals [1–3]. Unlike single-crystal samples and other highly oriented fibres, however, the copolymer is macroscopically isotropic and its Raman spectrum is independent of the direction of polarization of the incident laser beam. There was very little point-to-point variation in the spectra using the 2 μm spot size although the copolymer is, in fact, inhomogeneous at the microscopic ($< 1 \mu\text{m}$) level [15]. Fig. 2 shows the C \equiv C triple-bond stretching band before and after deformation to 1.5% strain. It indicates that the band shifts significantly to lower frequencies upon tensile

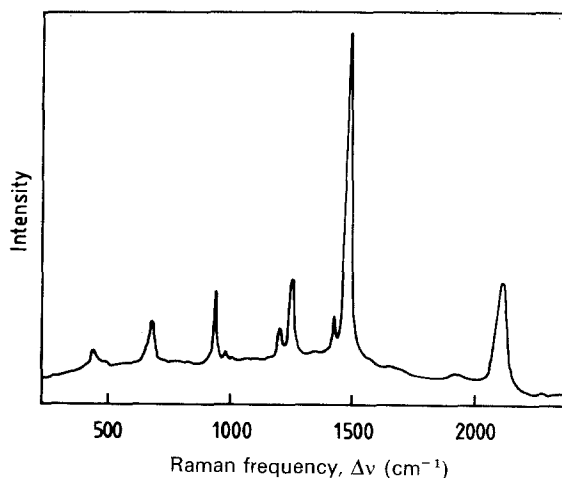


Figure 1 Raman spectrum of the diacetylene-containing copolymer.

deformation as the overall strain in the copolymer is transformed into the molecular deformation of polydiacetylene chains in the hard segments of the copolymer [16, 17]. Fig. 3 is a plot of the peak position of the Raman band, $\Delta\nu$, versus strain, ϵ , for the copolymer. There is a linear relationship up to 1.5% strain followed by a deviation from linearity at higher strain due probably to plastic deformation. In this particular copolymer, the strain dependence or strain sensitivity of Raman band $d\Delta\nu/d\epsilon = S$ was determined from the slope of the linear part of the curve in Fig. 3 and was found equal to $-5.3 \pm 0.4 \text{ cm}^{-1}/\%$. It has been found in earlier work [16, 17] that the value of $d\Delta\nu/d\epsilon$

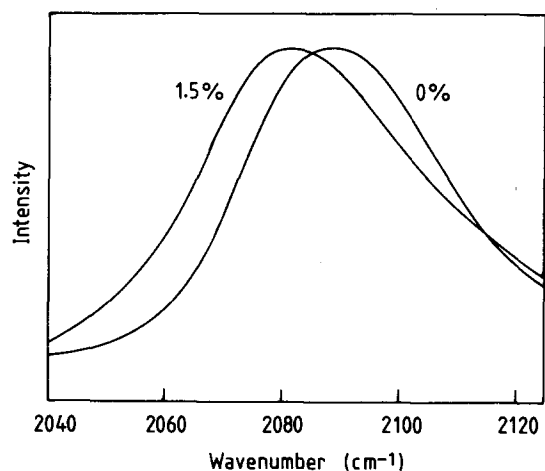


Figure 2 Raman bands of the 2090 cm^{-1} $\text{C}\equiv\text{C}$ triple-bond stretching mode before and after tensile deformation to 1.5% strain.

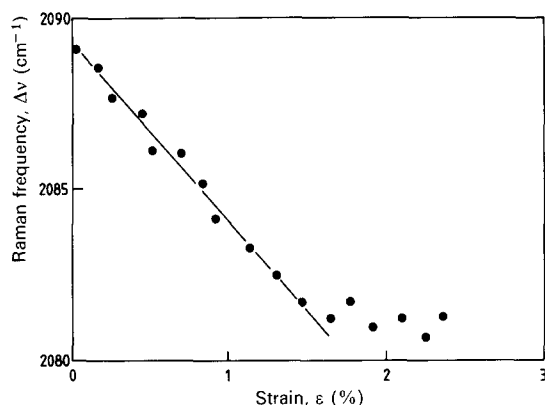


Figure 3 Strain dependence of Raman frequency of the $\text{C}\equiv\text{C}$ stretching band in the copolymer.

depends upon the structure of the copolymers. It was shown [16] that the composition used in this present study has the best combination of mechanical properties, Raman band intensity and strain-dependent Raman band shift, although copolymers with slightly higher strain sensitivities can also be prepared by varying the structure and morphology. Table I gives a list of strain sensitivities of the Raman-band frequencies for various types of materials. It can be seen that the value obtained from the diacetylene-containing copolymer, though smaller than the value for polydiacetylene single crystals, is considerably higher than those of less-oriented conventional polymers and is comparable to the values for highly oriented fibres such as aramids and gel-spun UHMW-PE fibres.

3.2. Analysis of the stress concentrations at defects

The dependence of the position of the Raman bands upon strain described above makes it possible to investigate stress concentrations around defects, such as holes or notches in the diacetylene-containing copolymer using Raman microscopy. Fig. 3 is essentially a strain gauge calibration curve for an optical strain gauge, because it relates the specimen strain to the frequency of the Raman band. It can be seen that there is an approximately linear relationship between the Raman frequency, $\Delta\nu$, and strain, ϵ , up to about 1.5% strain. Previous work [16] has shown that this linear relationship holds even for cyclic loading and unloading up to 1.5% strain but then breaks down when the copolymer is cycled to strains above this level. In the present study, holes and notches of known radii and length were introduced into cross-polymerized copolymer specimens. The stress concentration factors in the vicinity of the defects were determined experimentally by local strain measurement using Raman spectroscopy, and comparisons were made with the values calculated from theoretical stress analysis [18]. It was assumed that the specimens underwent only elastic deformation because in all the experiments, the tensile strain even in regions of stress (or strain) concentration was limited to $< 1.5\%$.

Fig. 4 illustrates two geometries of defects that have been investigated in this present work. The specimen is subjected to an overall applied stress (at a large distance from the defects) of σ_0 and there will be stress (or

TABLE I Peak frequency, $\Delta\nu$, and strain sensitivity, $S = d\Delta\nu/d\epsilon$, of the Raman bands of various materials

Materials	$\Delta\nu \text{ (cm}^{-1}\text{)}$	$d\Delta\nu/d\epsilon \text{ (cm}^{-1}/\%\text{)}^a$	Reference
Polydiacetylene single crystals	2080	- 20.0	[1-3]
Aramids	1613	- 4.4	[4-6]
UHMW-PE	1060	~ - 5	[7-9]
Rigid rods			
PBT	1477	- 12.1	[10]
PBO	1280	- 7.9	[11]
Conventional polymers			
Polypropylene	808	< - 1	[13, 14]
PET	1615	< - 1	[12]
Diacetylene-containing copolymers	2090	~ - 6	[16]

^a The data quoted are the highest values in the literature.

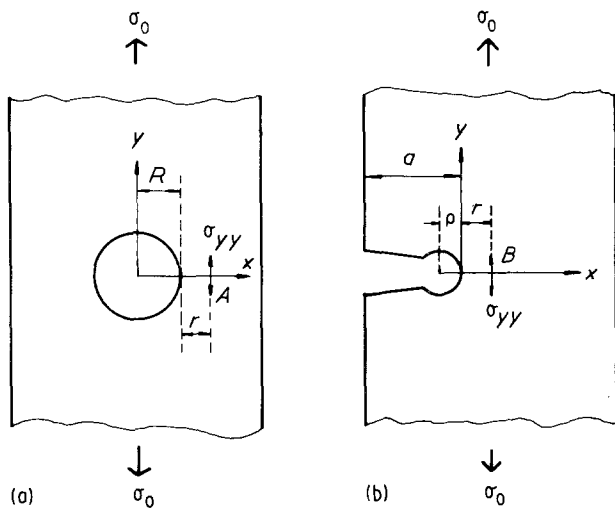


Figure 4 Geometries of defects in the copolymer specimen of finite width, W , subjected to a tensile stress of σ_0 in the y -direction. (a) Central hole of radius, R , (b) single-edge notch of length, a , and tip diameter, ρ .

strain) concentration at the equator of the hole and at the tip of the notch. The experimental stress concentration factor, F_E , is defined as the local stress divided by the overall applied stress in the bulk specimen, which is equivalent to the local strain divided by the overall strain in the elastic case. Because it has been shown in Fig. 3 that the strain-induced Raman frequency shift, $d\Delta\nu \propto d\varepsilon$, it follows that this frequency shift is a direct measure of the strain at the point of measurement. As the laser beam is polarized parallel to the tensile axis, the strain measured using Raman spectroscopy is the principal strain parallel to the direction of deformation. Hence, the measured stress concentration factors at positions A or B in Fig. 4 are given as

$$F_E = \frac{\sigma_{yy}}{\sigma_0} = \frac{\varepsilon_{yy}}{\varepsilon_0} = \frac{d\Delta\nu_{yy}}{d\Delta\nu_0} \quad (1)$$

where $\sigma_{yy}(\varepsilon_{yy})$ is the local tensile stress (strain) in the y -direction and $\sigma_0(\varepsilon_0)$ is the overall applied stress (strain), $d\Delta\nu_{yy}$ is the local Raman frequency shift at position A or B and $d\Delta\nu_0$ is the Raman frequency shift at positions far away from the defect area and hence free from stress concentrations (in all cases with the laser beam polarized parallel to the y -axis).

The measurement of Raman frequency shifts at points A and B and the pole of the hole (Fig. 4) were carried out at different strain levels, ε_0 , within the linear elastic region and the stress concentration factor, F_E , was determined using Equation 1. Fig. 5 shows the dependence of the Raman frequencies, $\Delta\nu$, upon the overall strain, ε_0 , in the copolymer at the three different positions of stress concentration. The strain-induced Raman frequency shift at the position far away from the defects was about $-5 \text{ cm}^{-1}/\%$ strain and similar to that for an unnotched specimen (Fig. 3). A larger shift in terms of $d\Delta\nu/d\varepsilon$ ($-16 \text{ cm}^{-1}/\%$ strain) was found near the equator of a circular hole although no significant shift was observed at the pole. A considerably larger shift of $-33 \text{ cm}^{-1}/\%$ strain was obtained ahead of a notch

tip. These observations are obviously due to different levels of stress concentration around different defects. A number of specimens with various defect geometries and dimensions were tested and the results are summarized in Table II.

Theoretical predictions of the stress concentration factors were obtained using conventional stress analysis expressions [18]. For a plate of finite width with a central circular hole, the theoretical stress concentration factor in the plate along the equator of the hole, F_T , is given by [18]

$$F_T = \frac{\sigma_{yy}}{\sigma_0} = \frac{k}{2} \left[2 + \left(\frac{R}{R+r} \right)^2 + 3 \left(\frac{R}{R+r} \right)^4 \right] \quad (2)$$

where k is a finite width correction parameter, R is the radius of the hole and r is the distance along the equator from the edge of the hole. For a single-edge notched plate of finite width, F_T is given as [18]

$$F_T = \frac{\sigma_{yy}}{\sigma_0} = \frac{ka^{1/2}}{(2r)^{1/2}} \left(\frac{1 + \frac{\rho}{r}}{1 + \frac{\rho}{2r}} \right)^{3/2} \quad (3)$$

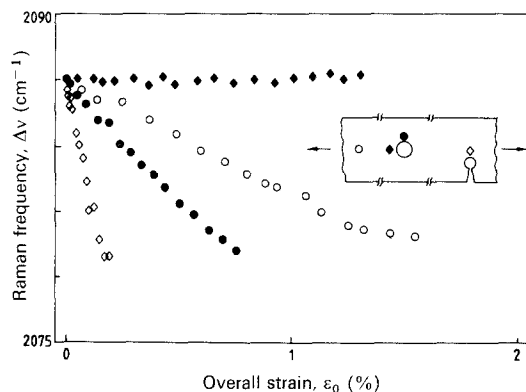


Figure 5 Plots of Raman frequencies measured at the positions of different stress concentration conditions indicated in the sketch versus overall strain in the specimen: (○) far away from the defects, (●) near the equator of a circular hole, (◆) at the pole, (◇) ahead of a notch tip.

TABLE II Stress concentration factors ahead of the equator of the circular holes and notch tips in the copolymer specimen of width, W . The geometric parameters are defined in Fig. 4

	a (mm)	ρ (mm)	W (mm)	r (mm)	F_T	F_E
Hole	1.5 ^a	—	10.01	0.1	2.34	2.06
Hole	1.5 ^a	—	10.25	0.1	2.34	2.07
Notch	3.79	0.2	10.03	0.28	5.67	4.78
Notch	3.68	0.4	10.20	0.2	6.22	6.59
Notch	3.55	0.6	10.42	0.11	6.64	5.90
Notch	3.41	0.6	10.67	0.24	6.05	4.84
Notch	3.74	0.8	10.28	0.2	5.73	6.02
Notch	3.75	1.0	10.08	0.26	5.16	4.38
Notch	3.75	1.0	10.08	0.40	4.45	4.12

^a Hole radius, R .

assuming that $\rho \ll a$ and $r \ll a$. The constant k is again a finite width correction factor, a is the crack length, ρ is the notch tip radius and r is the distance ahead of the notch tip along the centre line of the notch. The finite width correction factors for both central holes and single-edge notched plates deformed in tension may be obtained from Williams [18].

Fig. 6 is a plot of F_E versus F_T and shows that the experimentally measured stress concentration factors are in reasonable agreement with the values calculated by the theoretical stress analyses [18]. The scatter in the data may be attributed to difficulties in determining the exact geometry of the notch tip under the microscope and errors introduced from the measurement of the distance ahead of crack or notch tips. The systematic underestimation of F_E may be due to yielding taking place in the areas of high stress concentration and thereby reducing the stress concentration. There may also be errors caused by the approximations in the theoretical analyses [18] such as the estimation of the finite width correction factor and the assumption that $\rho \ll a$, etc.

In separate experiments, point-to-point measurements were made of the Raman frequency shifts as a function of the distance, r , away from the edge of a hole and ahead of the notch tip along the x -axis defined in Fig. 4. The measurements were made with the overall strain kept constant at 0.42% for measurements around the centre hole and at 0.16% in the case of the single-edge notch. The results in Fig. 7 show that the Raman frequency increases and then levels off as the distance from the equator of the hole or the distance ahead of the notch tip, r , is increased. This indicates the decay of the tensile stress concentration as the distance from the defect is increased. The strain value at each point can be calculated using the calibration of the strain dependence of the Raman frequency, S , which is $-5.3 \text{ cm}^{-1}/\%$ strain for this

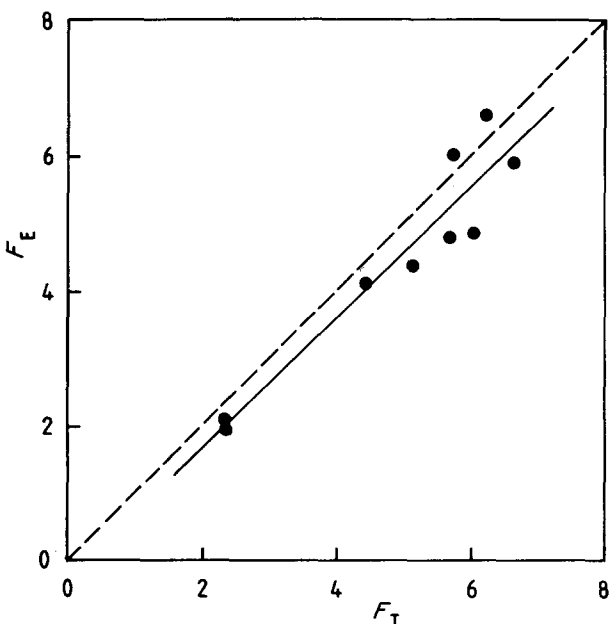


Figure 6 Plot of the Raman-measured stress concentration factors, F_E , versus theoretical values, F_T . (---) $F_E = F_T$, (—) least squares fit of the data.

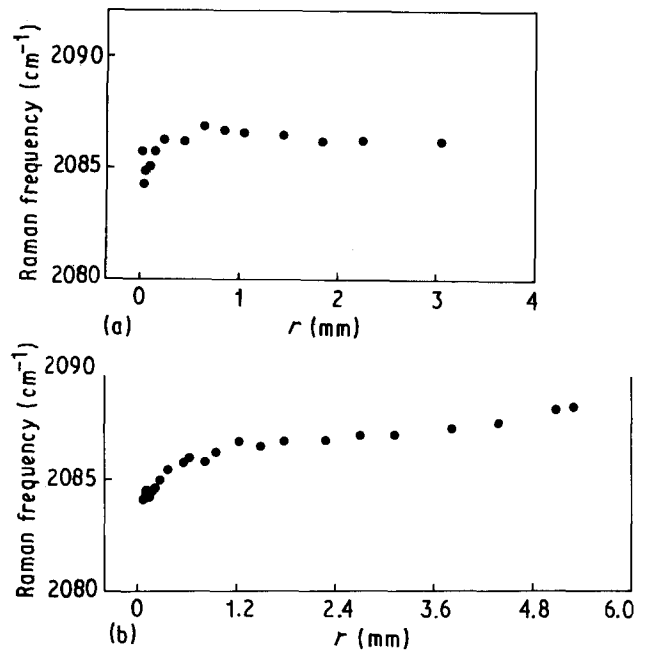


Figure 7 Peak Raman frequency, $\Delta\nu_{yy}$, versus the distance, r , ahead of (a) the equator of the central circular hole subject to an overall strain ϵ_0 of 0.42%, and (b) the tip of the single-edge notch for a plate subjected to an overall strain ϵ_0 of 0.16%.

material (Fig. 3). Fig. 8 gives the plot of the Raman-measured strains as a function of the distance. The variation of the tensile strain with distance, r , for a central hole in a flat plate is given as [18]

$$\epsilon = \frac{k\epsilon_0}{2} \left[2 + \left(\frac{R}{R+r} \right)^2 + 3 \left(\frac{R}{R+r} \right)^4 \right] \quad (4)$$

and for a single-edge notch as [18]

$$\epsilon = \frac{k\epsilon_0 a^{1/2}}{(2r)^{1/2}} \frac{\left(1 + \frac{\rho}{r} \right)}{\left(1 + \frac{\rho}{2r} \right)^{3/2}} \quad (5)$$

The experimental data are seen to follow the same trends as predicted by Equations 4 and 5, although the agreement with the theory is not exact. The deviations between experiment data and theory are again due mainly to difficulties in defining r and the crack and notch tip radii. Errors may also arise from the approximations in the theoretical calculations such as the assumption of no bending in the specimen and the approximation in the finite width correction [18]. Furthermore, slight plastic deformation may occur at the high stress concentrations at the equator of the hole and the crack tip which leads to deviation from the linear elastic assumption. Nevertheless, it can be seen from Fig. 8 that the Raman technique is an excellent method of determining strain or stress distributions at defects.

Another experiment was also carried out to map the strain field around a single-edge notch in a deformed copolymer tensile specimen in which there was an overall strain of 0.16% ($d\Delta\nu = -0.85 \text{ cm}^{-1}$). Fig. 9 illustrates the Raman band frequencies at different positions in the vicinity of the notch tip. Measurements were made as a function of r along the dotted

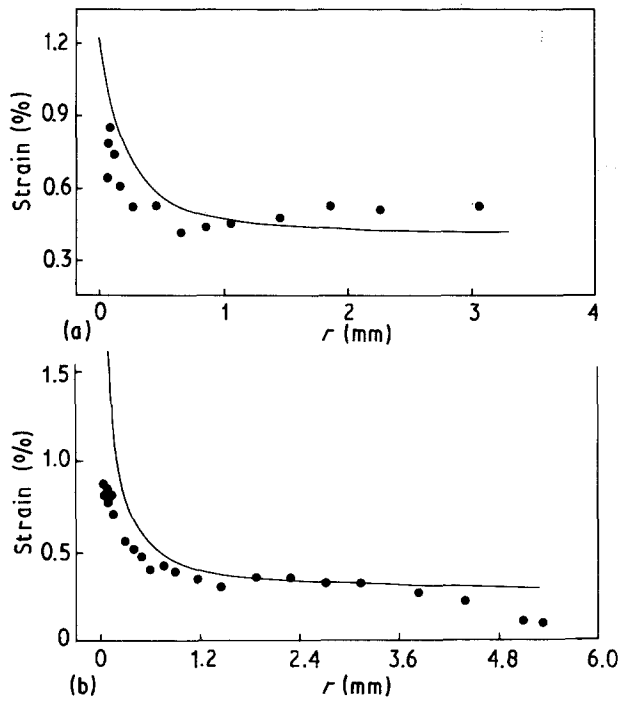


Figure 8 Strain distributions ahead of (a) the equator of a central plate hole, and (b) the tip of a single-edge notch. The solid lines are theoretical predictions from stress analysis (Equations 4 and 5).

lines parallel to the x -axis and the centre line of the notch but at different positions along y as indicated in sketches in Fig. 9. As expected, a higher level of tensile strain is observed near the notch tip which manifests itself as large negative shift of Raman frequency shown in Fig. 9a ($y = 0$) and b ($y = 0.18$ mm). For these small values of y (i.e. close to the centre-line of the notch) the tensile strain decreases rapidly in the range $0 \leq r \leq 0.5$ mm, then gradually reaches a constant value in the range $1.0 \text{ mm} \leq r \leq 3.0$ mm and increases further as $r > 3$ mm. This gradual reduction in tensile strain for $r > 3$ mm is not predicted by Equation 5 which is valid only when $\rho \ll a$ and $r \ll a$ which do not apply in this case. It is possible that some compression developed with increasing r , perhaps due to bending in the specimen of finite width, and hence reducing the effect of the stress concentration. This effect is observed to be similar for all four values of y at which measurements were made. This is difficult to predict accurately using classical stress analysis and numerical stress analysis and numerical methods such as finite element analysis would have to be used instead. Such an approach is beyond the scope of this present paper.

Interesting results were also obtained when the strain measurements were made along lines at positions further from the notch tip ($y = 0.46$ mm and $y = 0.60$ mm). As shown in Fig. 9c and d, the strain first increases to a maximum value and then decreases to a constant value before decreasing further as $r > 3$ mm. Again an accurate theoretical prediction is very difficult to achieve in such a situation.

Fig. 10 shows the variation of $\Delta\nu$ and hence ϵ_{yy} with y for $x = 0$ (i.e. in line with the notch tip). It can be seen that the strain ϵ_{yy} decreases steadily with distance from the notch tip as the effect of the stress concentration decreases. The results in Figs 9 and 10 show the

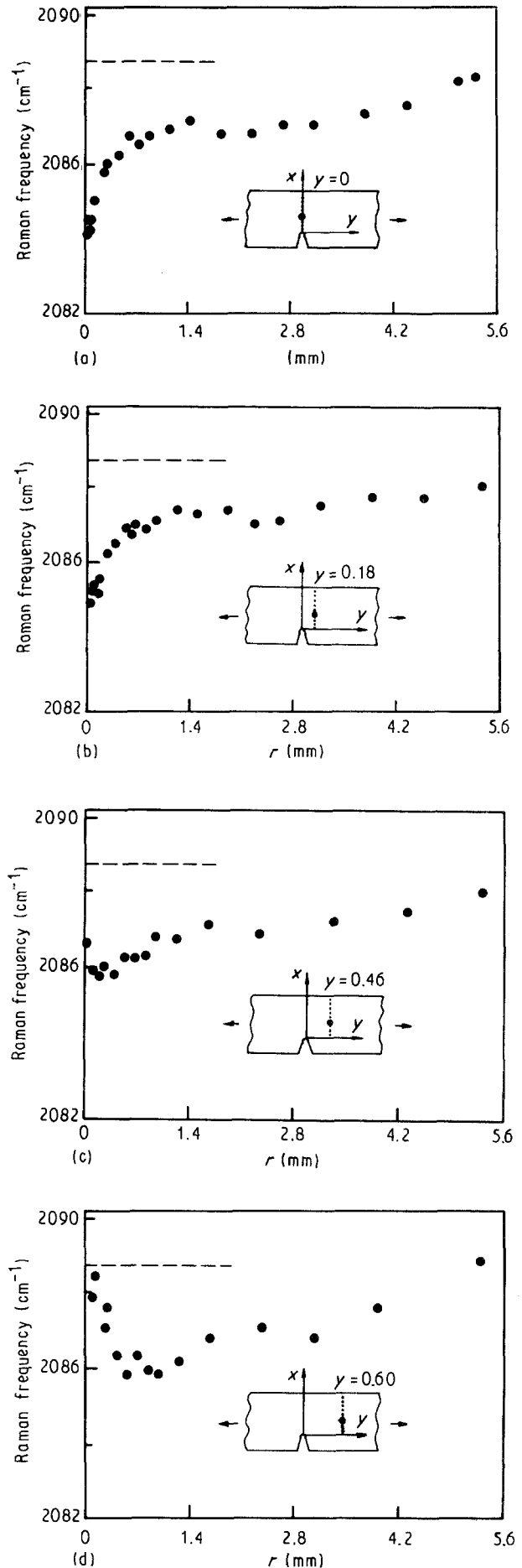


Figure 9 Raman frequency distribution at different positions indicated in the sketches near a single-edge notch tip (0.60 mm radius) in a deformed copolymer specimen. The overall strain was 0.16%. (---) the Raman frequency of the sample under strain-free conditions.

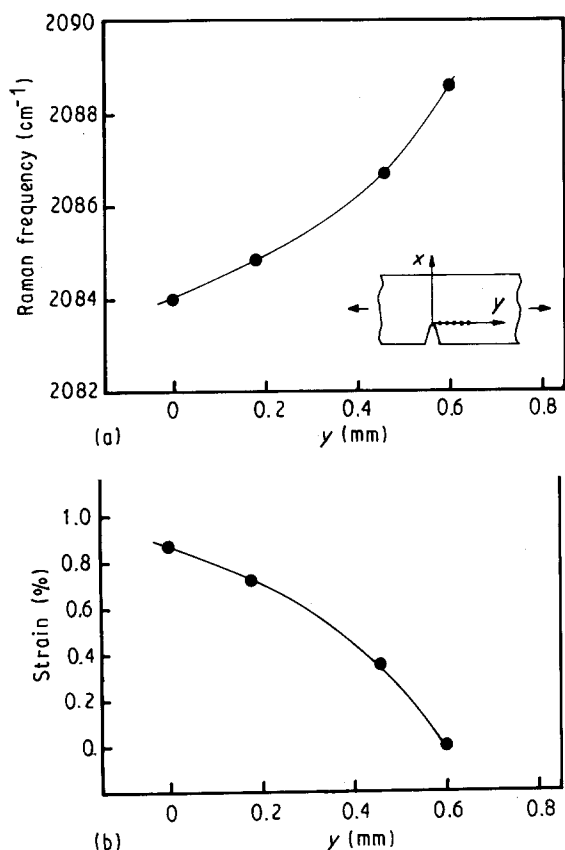


Figure 10 (a) Variation of Raman Frequency with distance from the notch tip along the y -axis for an overall strain, ϵ_0 , of 0.16%. (b) Variation of strain, ϵ_{yy} , with distance along the y -axis determined from the data in (a).

potential of Raman spectroscopy for measuring strain in complex stress fields such as in the vicinity of notches or cracks.

4. Conclusion

Rigid diacetylene-containing copolymers are optically strain sensitive. The strain sensitivities of their Raman bands are at least comparable to those of highly oriented fibres, such as aramids and rigid rod polymers. This enables point-to-point variations of strain to be measured by monitoring the Raman frequencies in the copolymers.

Stress concentrations around defects in copolymer specimens have been studied using Raman microscopy. The point-to-point strain measurement or strain mapping in the vicinity of defects in the copolymer was achieved because of the high spatial resolution ($\approx 2 \mu\text{m}$) of the Raman microscope. The experi-

mental data were found to agree reasonably well with theoretical predictions using conventional stress analysis and also provided additional information which is difficult to predict by theories.

Another advantage of the copolymers is their ease of being processed into various shapes and forms. In particular, they can be used as strain-sensitive surface coatings [16] and strain-sensitive composite matrices. The diacetylene-containing copolymers clearly represent a new class of optical strain sensors which will have a wide range of applications in stress or strain analysis.

Acknowledgement

This work was supported by a research grant of the SERC.

References

1. D. N. BATCHELDER and D. BLOOR, *J. Polym. Sci. Polym. Phys. Ed.* **17** (1979) 569.
2. C. GALIOTIS, R. J. YOUNG and D. N. BATCHELDER, *ibid.* **21** (1983) 2483.
3. G. WU, K. TASHIRO and M. KOBAYASHI, *Macromolecules* **22** (1989) 188.
4. S. van der ZWAAG, M. G. NORTHOLT, R. J. YOUNG, I. M. ROBINSON, C. GALIOTIS and D. N. BATCHELDER, *Polym. Commun.* **28** (1987) 276.
5. C. GALIOTIS, I. M. ROBINSON, D. N. BATCHELDER and R. J. YOUNG, in "Engineering Applications of new Composites", edited by S. A. Paipetis and G. C. Papanicolaou (Omega, Wallingford, 1988) p. 409.
6. R. J. YOUNG, D. LU, R. J. DAY, H. DAVIS and W. KNOFF, *Polymer*, *in press*.
7. K. TASHIRO, G. WU and M. KOBAYASHI, *Polymer* **29** (1988) 1768.
8. K. PRASAD and D. T. GRUBB, *J. Polym. Sci.* **B27** (1989) 381.
9. B. J. KIP, M. C. P. van EIJK and R. J. MEIER, *ibid.* **B29** (1991) 99.
10. R. J. DAY, I. M. ROBINSON, M. ZAKIKHANI and R. J. YOUNG, *Polymer* **28** (1987) 183.
11. R. J. YOUNG, R. J. DAY, M. ZAKIKHANI, *J. Mater. Sci.* **25** (1990) 127.
12. L. J. FINA, D. I. BOWER and I. M. WARD, *Polymer* **29** (1988) 2146.
13. R. A. EVANS and H. E. HALLAM, *ibid.* **17** (1976) 838.
14. R. P. WOOL and R. H. BOYD, *J. Appl. Phys.* **51** (1980) 5116.
15. X. HU, J. L. STANFORD, R. J. DAY and R. J. YOUNG, *Macromolecules*, **25** (1992) 672.
16. *Idem*, *ibid.* **25** (1992) 684.
17. R. J. DAY, J. L. STANFORD and R. J. YOUNG, *Polymer* **32** (1991) 1713.
18. J. G. WILLIAMS, "Stress Analysis of Polymers" (Longman, London, 1973) p. 225.

Received 18 December 1991
and accepted 23 January 1992